

Chapter 2

Phanerozoic Life and Mass Extinctions of Species

Falling Star

*For an infinitely long second, nascent
Your tail plots a crescent, a fiery arc
From a star-spangled sky incandescent
To the fast sleeping Earth, in the dark
Your grave for all time.*

*Who are you, friend or foe, stranger
Fragment fallen by a space highway
Of the asteroid belt, posing danger
Or some orbit-decayed fancy hardware
Of fatal star wars fleets?*

*Are you a harbinger of good news
Or signal dire distress
For this embattled Earth, in its blues
Will your fleeting torch impress
A new truth?*

*Will you plunge way beyond yonder
Or fall here, close by my side
On this red desert dune, I wonder
Stranded tonight, wide eyed
In awe, without faith?*

(By Andrew Glikson)

Abstract Early conflicts between uniformitarian and gradual theories of evolution (James Hutton 1726–1797; Charles Lyell 1797–1875) and catastrophic theory (Georges Cuvier 1769–1832) have been progressively resolved by advanced paleontological, sedimentary, volcanic and asteroid impact studies and by paleo-climate studies coupled with precise isotopic age determinations, indicating periods of gradual evolution were interrupted by abrupt events which have transformed the habitat of plants and organisms and resulted in mass extinction of species. Detailed investigations of the carbon, oxygen and sulphur cycles using a range of proxies, including leaf pore stomata, $\delta^{13}\text{C}$, $\delta^{34}\text{S}$ and $^{87/86}\text{Sr}$ isotopes, as well as geochemical mass balance modeling, provide detailed evidence of major trends as well as distinct events in the atmosphere–ocean–land system during the Paleozoic and Mesozoic eras (542–65 Ma), including greenhouse Earth periods ($\text{CO}_2 \sim 2,000\text{--}5,000$ ppm)

and glacial phases ($\text{CO}_2 < 500$ ppm), with implications for biological evolution. The Cenozoic era includes four components (A) post K-T impact warming culminating with the Paleocene-Eocene hyperthermal at ~ 55 Ma; (B) long term cooling ending with a sharp temperature plunge toward formation of the Antarctic ice sheet from 32 Ma; (C) a post-32 Ma era dominated by the Antarctic ice sheet, including limited thermal rises in the end-Oligocene, mid-Miocene and end-Pliocene, and (D) Pleistocene glacial-interglacial cycles. Hominin evolution in Africa occurred during a transition from tropical to dry climates punctuated by alternating periods of extreme orbital forcing-induced glacial-interglacial cycles, suggesting variability selection of Hominins.

The geological record betrays a close correspondence between paleontological, sedimentary, volcanic, asteroid impact and paleo- CO_2 and paleo-temperature trends, allowing identification of environmental factors which underlie the evolution and extinction of species (McElwain et al. 1999; McElwaine and Punyasena 2007; Beerling 2002a, b; Beerling et al. 2002; Keller 2005; Glikson 2005). Five major mass extinction events and several moderate extinction events have affected the evolution of marine invertebrates (Fig. 2.1). High-resolution regional palaeoecological studies indicate extensive ecological upheaval, high species-level turnover and recovery intervals lasting millions of years, with close correlations to upheavals affecting terrestrial vegetation (McElwain and Punyasena 2007).

When a large (>200 meters) asteroid hits a solid surface at a high angle it penetrates to a depth of approximately $\times 1.5$ times its diameter, depending on the rheology of the impacted rocks, where its kinetic energy is translated into heat, triggering an explosion, fragmentation, cratering, melting and vaporization of the immediately surrounding rocks. In craters larger than about 4 km the Earth's crust rebounds to form a central uplift (French 1998; Glikson 2013). Depending on the size of the impact, seismic waves propagate, leading to earthquakes, faulting and tsunami waves over large regions. Environmental effects of asteroid impacts include the initial fireball flash, mega-tsunami waves, release of aerosols (dust, sulphur dioxide, carbon soot), acid rain and release of greenhouse gases (water, CO_2 , methane, Nitrous oxide) from cratered regions, leading to ocean acidification. This leads to an asteroid winter phenomenon, with some 10–20 % of solar radiation blocked for 8–13 years (Pope et al. 1997), followed by a greenhouse-gas induced warm period lasting centuries to millennia. Species which have escaped the immediate regional and transient effects of large impacts were affected by the long-lasting consequences of the well-mixed greenhouse gases, mainly CO_2 , Nitrous oxide and methane. CO_2 stays in the atmosphere for thousands to tens of thousands years, leading to extended periods of high global temperatures, compounding the effects on the biosphere. Effects on the oceans include acidification, anoxia (oxygen solubility decreasing with higher temperatures) and consequent anoxic conditions and toxic H_2S forming emanations (Ward 2007).

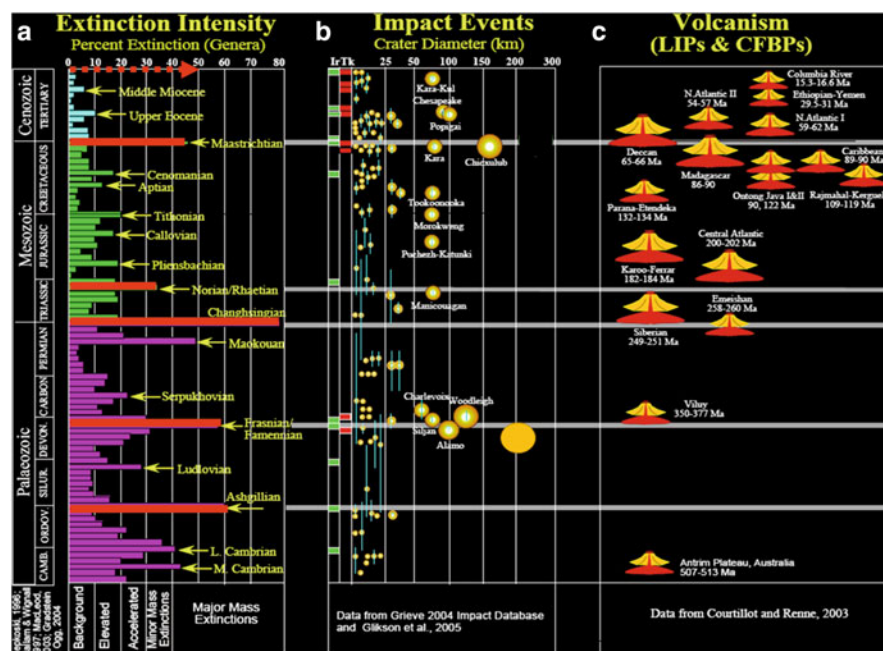


Fig. 2.1 Phanerozoic mass extinctions, asteroid impacts, and large igneous provinces. **(a)** Extinction intensity; **(b)** Impact events; **(c)** Volcanism. Stratigraphic subdivisions and numerical ages are after Gradstein and Ogg (2004). The extinction record is based on genus-level data by Sepkoski (1996). The number of impact events, size and age of craters follows largely the Earth Impact Database (2005), with modification by AG (Courtesy G. Keller)

Phanerozoic mass extinctions marked by carbon and oxygen isotopic anomalies include the End-Ordovician (Marshall 1992; Marshall et al. 1997; Brenchley et al. 2003), Late Devonian (Stephens and Sumner 2002), Permian-Triassic boundary, Late Triassic and K-T boundary (Maruoka et al. 2007). Changes in the carbon cycle recorded by total organic carbon (TOC) and stable carbon isotope ratios ($\delta^{13}\text{C}_{\text{carb}}$ and $\delta^{13}\text{C}_{\text{org}}$) constitute sensitive fingerprints of mass burial of organic matter derived from marine organisms, fallout from forest fires, or increased biological productivity. Variations in oxygen isotope ratios ($\delta^{18}\text{O}$) reflect changes in ice volumes and salinity. Marked changes in these parameters accompany major volcanic eruptions, asteroid impacts (Maruoka et al. 2007) and methane release (Zachos et al. 2008) (Fig. 1.23).

Positive excursions in both $\delta^{18}\text{O}$ and $\delta^{13}\text{C}_{\text{carb}}$ at the end-Ordovician signify parallel decrease in temperature and in biological productivity at the onset of 443.4 ± 1.5 Ma Ashgill/Hirnatian glaciation and extinction event (Marshall 1992; Marshall et al. 1997; Brenchley et al. 2003). A global nature of the glaciation is indicated from the widespread positive carbon isotope, including $\delta^{13}\text{C}_{\text{carb}}$ and $\delta^{13}\text{C}_{\text{org}}$.

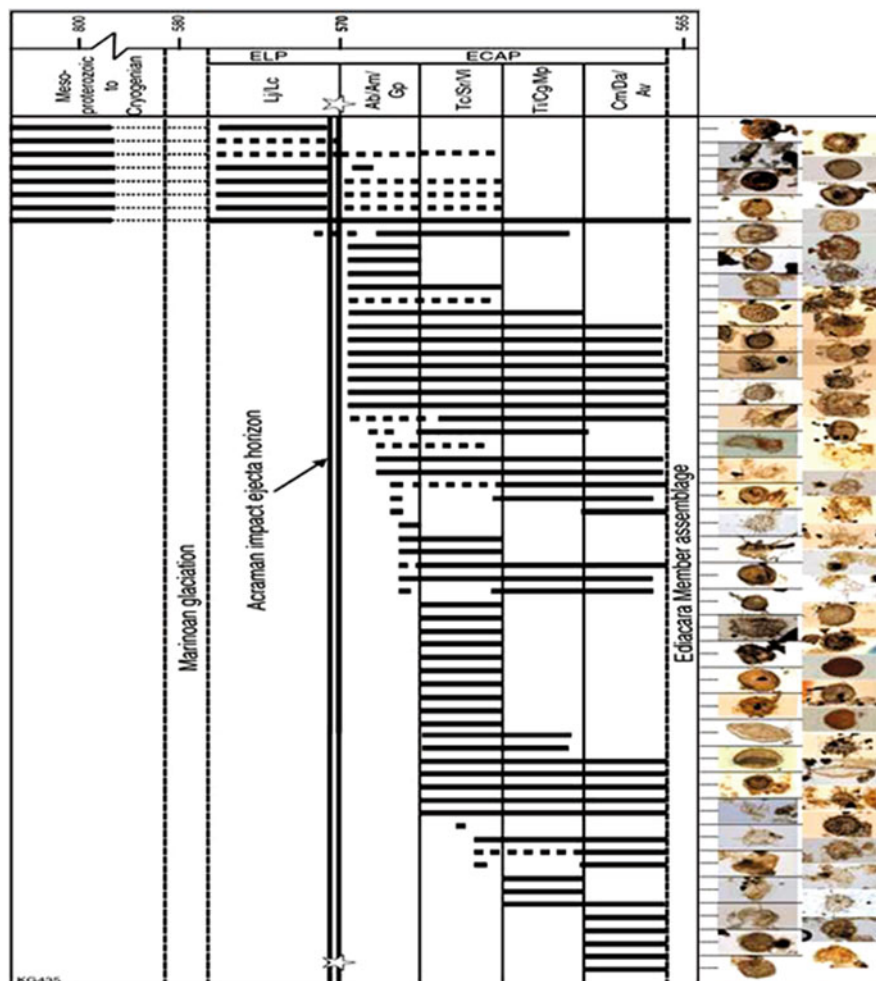


Fig. 2.2 Stratigraphic distribution of Acritarchs following the Marinoan glaciation at ~580 Ma, displaying a major discontinuity at ~570 Ma coinciding with ejecta from the Acraman impact event, followed by major radiation (Grey 2005; Courtesy K. Grey. Image courtesy of the Geological Survey of Western Australia, Department of Mines and Petroleum, State of Western Australia 2013. ELP – Ediacaran Leiosphere Palynoflora; ECAP – Ediacaran Complex Acanthomorph Palynoflora)

and oxygen isotope shifts measured from Brachiopod shells over a wide range of paleo-latitudes. Upper Ordovician cores from Estonia and Latvia record a $\delta^{13}\text{C}_{\text{carb}}$ shift of up to 6‰ and similar profiles were measured in Nevada, suggesting a global chronostratigraphic signal (Brenchley et al. 2003). Positive correlation between $\delta^{13}\text{C}$ and $\delta^{18}\text{O}$ militates for genetic relations between biological activity and temperature (Figs. 2.3, and 2.4).

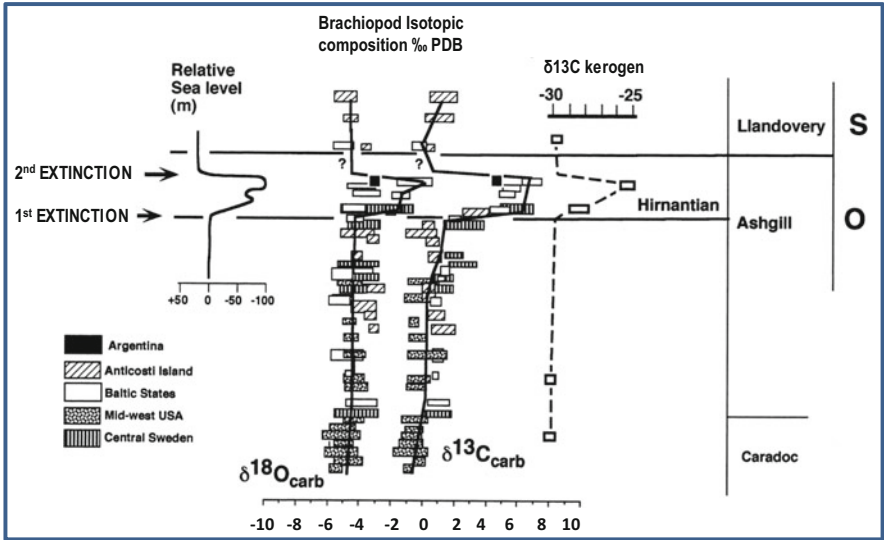


Fig. 2.3 Summary diagram showing the relationships between biological, bathymetric and stable isotopic changes in the late Ordovician. The marked positive carbonate isotopic excursion in the early Hirnantian is paralleled by a shift in the isotopic composition of organic carbon. Data from Argentina demonstrate elevated $\delta^{13}\text{C}$ in brachiopods from high palaeolatitudes but the oxygen values should be regarded as a minimum because even the least-altered sample showed signs of diagenetic alteration (Marshall et al. 1997; Elsevier, by permission)

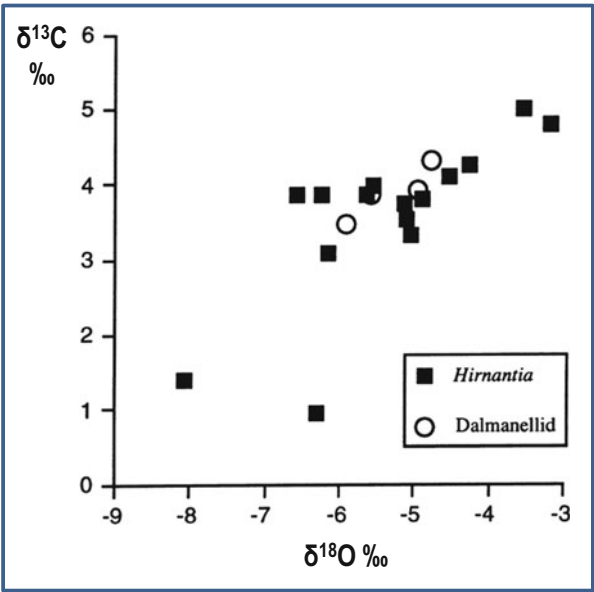


Fig. 2.4 The relations between organic matter-related $\delta^{13}\text{C}$ and temperature related $\delta^{18}\text{O}$ stable isotope proxies in Ordovician brachiopod samples from the La Pola and Don Braulio sections (Marshall et al. 1997; Elsevier, by permission)

Upper Devonian isotopic excursions were studied at the Fitzroy reef complex of the Canning Basin, Western Australia, where well-exposed continuous Frasnian-Fammenian sequences record interactions between sea level changes, sediment supply, ocean chemistry, and paleoecology (Stephens and Sumner 2002). The Frasnian-Fammenian transition correlates with positive $\delta^{13}\text{C}$ shifts, consistent with similar intervals of the Kellwasser horizons in Europe (Figs. 2.5 and 2.6). By analogy to the end-Ordovician, an overall positive correlation pertains between $\delta^{13}\text{C}$ and $\delta^{18}\text{O}$ relations (Fig. 2.7), suggesting a decline in biological productivity with lower temperatures (Stephens and Sumner 2002). Likely connections between the Frasnian-Fammenian (~374 Ma) and End-Devonian (~359 Ma) mass extinctions (Fig. 2.1, and 2.6) and asteroid impacts (Woodleigh, Western Australia ~359 \pm 4 Ma; Siljan, Sweden, 376.8 \pm 1.7 Ma; Charlevoix, Quebec, 342 \pm 15; Alamo, New Mexico, ~360 Ma) (Glikson 2005; Keller 2005) remain to be established once the relations between the stratigraphic context of fallout/ejecta units of these impact is studied.

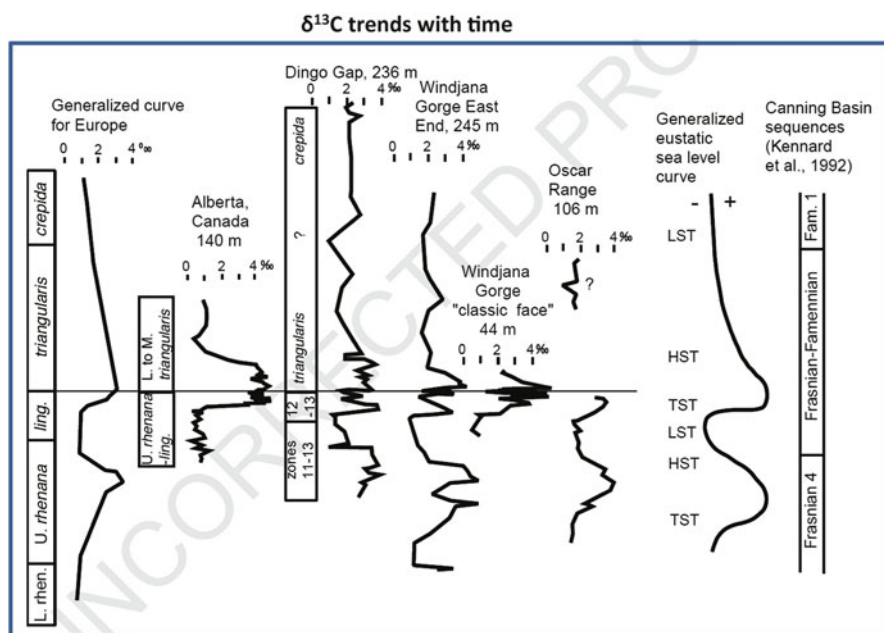


Fig. 2.5 $\delta^{13}\text{C}$ rises representing decline in biological activity following the Frasnian-Fammenian mass extinction. The trends from Canning Basin compared to generalized carbon isotope curve from Europe and carbon isotope curve from Canada. The $\delta^{13}\text{C}$ curve from Europe is plotted against time. The $\delta^{13}\text{C}$ curves from Australia and Canada are plotted against thickness and adjusted so conodont dates correlate with the European section. Gap in Oscar Range curve is due to unconformity. The generalized eustatic sea level curve is interpreted from Canning Basin and European sections and agrees with Hallam and Wignall's (1997) interpretation (Stephens and Sumner 2002; Elsevier, by permission)

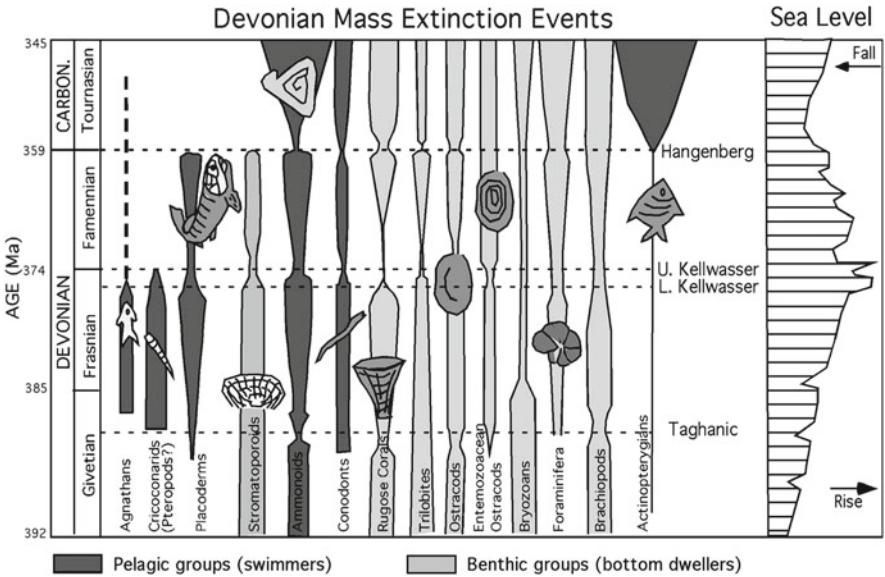


Fig. 2.6 Biotic effects of Devonian mass extinction events (Hallam and Wignall 1997). Major mass extinctions are in the lower and upper Kellwasser at the end of the Frasnian, decimating reef system, shallow benthic fauna and pelagic swimmers. The crises were associated with sea-level rises, warm climate and widespread ocean anoxia. The Hangenberg extinction affected mainly pelagic groups including ammonoids and fish. The mid-Devonian Taghanic extinction was part of a long-term diversity decline (after Keller 2005; Australian Journal of Earth Science, by permission)

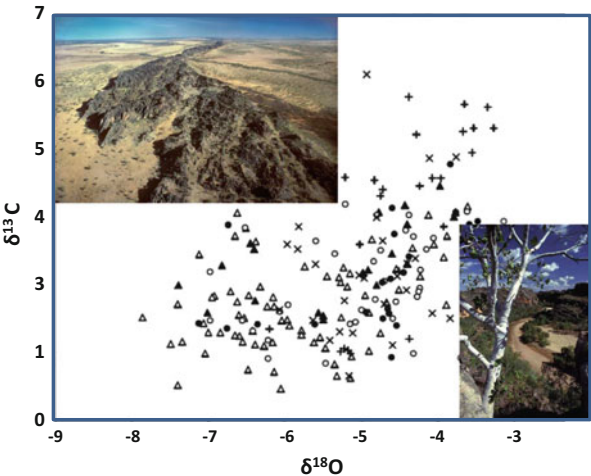


Fig. 2.7 Carbon and oxygen isotopic values of samples used for $\delta^{13}\text{C}$ correlations (Stephens and Sumner 2002; Elsevier, by permission). Photographs: top left – Napier Range, Kimberley (courtesy Reg Morrison; bottom right – Windgina Gorge, Kimberley (Courtesy Reg Morrison)

A marked decline of between 4‰ and 7‰ $\delta^{13}\text{C}$ values straddling the Permian-Triassic boundary (251 Ma), associated with sharp fluctuation of CO_2 (Fig. 2.8), represents world-wide deposition of extinct biota high in ^{12}C (Ward 2007; Korte and Kozur 2010) (Figs. 2.9 and 2.10). Low $\delta^{13}\text{C}$ values lasted over about 0.5 million years, beginning in the Changhsingian (253.8 ± 0.7 Ma) and reaching a first minimum at the P-T boundary (251 ± 0.4 Ma). The trend is interrupted by two short-term positive excursions following which a decline in $\delta^{13}\text{C}$ values continues. Korte and Kozur (2010) interpret these variations in terms of (1) direct and indirect effects of volcanism of the Siberian Traps; (2) anoxic deep waters occasionally reaching very shallow sea levels. The authors question an abrupt release of isotopically light methane from sediments or permafrost soils as a source for the negative carbon-isotope trend. With near to 80 % mass extinction of genera (Keller 2005), a prolonged recovery of the biosphere followed over a period of near to 5 million years (Erwin 1994, 2006; Korte and Kozur 2010).

Oxygen isotope ratios measured on phosphate-bound oxygen in conodont apatite from South China decrease by 2‰ in the latest Permian, translating into low-latitude surface water warming of 8 °C (Joachimski et al. 2012). The oxygen excursion coincides with a negative $\delta^{13}\text{C}_{\text{carb}}$ shift, suggesting CO_2 emission by Siberian Trap volcanism constituted a factor driving warming. Temperature rise commenced immediately prior to the main extinction phase, with maximum temperatures documented in the latest Permian at Meishan (bed 27), coinciding with the main pulse of extinction and the collapse of marine and terrestrial ecosystems. Prolonged warming through the Early Triassic may have played a major role in the delayed recovery in the aftermath of the Permian-Triassic crisis.

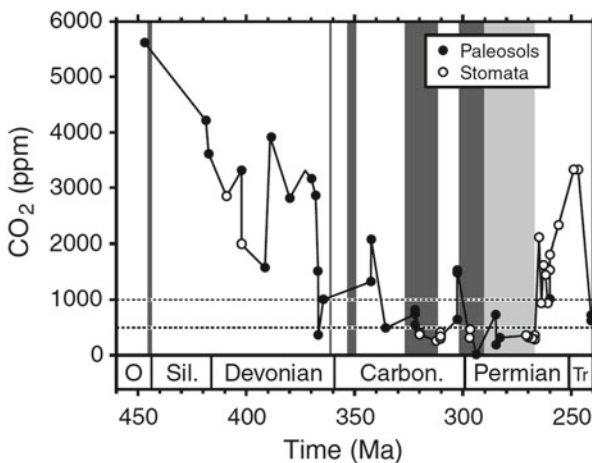


Fig. 2.8 CO_2 and temperature records for the Late Ordovician to early Triassic (460–240 Ma) (Royer 2006; Elsevier, by permission). Note the upper to late Devonian and Permian-Triassic boundary peaks of ~3000 ppm CO_2 , corresponding to a major mass extinction of species

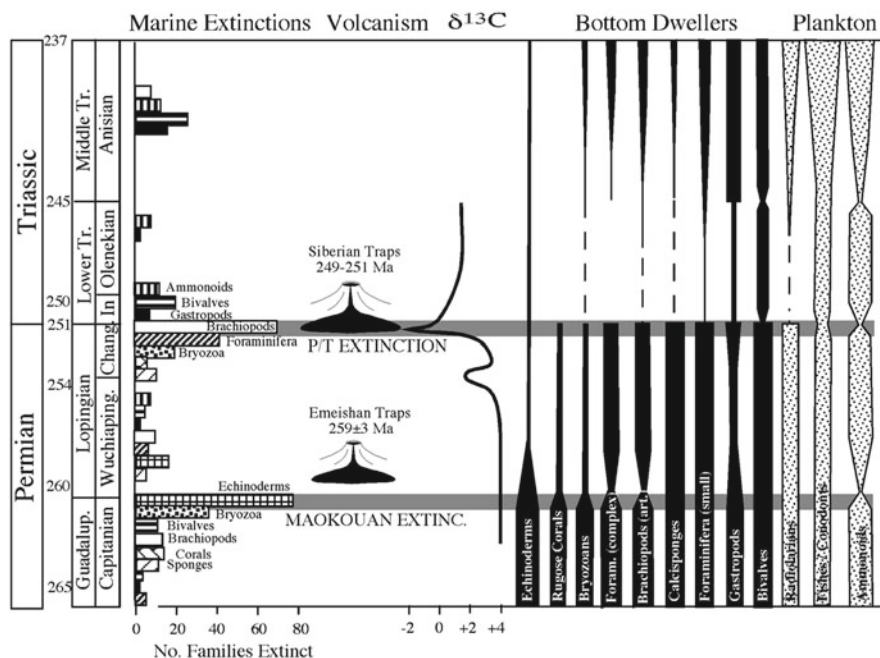


Fig. 2.9 Faunal turnover, impacts and volcanism across the Permian – Triassic transition. Faunal data modified after Hallam and Wignall (1997); volcanism after Courtillot and Renne (2003). (Keller 2005; Australian Journal of Earth Science, by permission)

The end-Triassic extinction at 201.4 Ma, associated with opening of the Central Atlantic Magmatic Province (CAMP), is marked by large negative carbon isotope excursion, including a transient increase in CO_2 (Fig. 2.11). Carbon isotopic anomalies of leaf wax derived lipids (n-alkanes), wood, and total organic carbon from lacustrine sediments intercalated with CAMP volcanics in eastern North America are similar to anomalies in sections across the Atlantic, suggesting synchronous onset of the extinction (Whiteside et al. 2010). The onset of the anomalies precedes the oldest basalts in eastern North America but is simultaneous with the eruption of the oldest flows in Morocco, signifying a CO_2 super greenhouse and marine acidification crisis. Bachan et al. (2012) report $\delta^{13}\text{C}_{\text{carb}}$ excursions coincident with the disappearance of the Triassic fauna and two overlying positive excursions (Fig. 2.12). No negative $\delta^{13}\text{C}_{\text{org}}$ were recorded, suggesting diagenetic alteration of organic matter. The data suggest perturbation of the global carbon cycle persisting for substantial lengths of geologic time following the mass extinction (Fig. 2.13).

The most extensively studied asteroid impact boundary of the 65 Ma K-T event has yielded definitive carbon, oxygen and sulphur isotopic values diagnostic of the geological, geochemical and biological effects of large-scale impact. Detailed studies

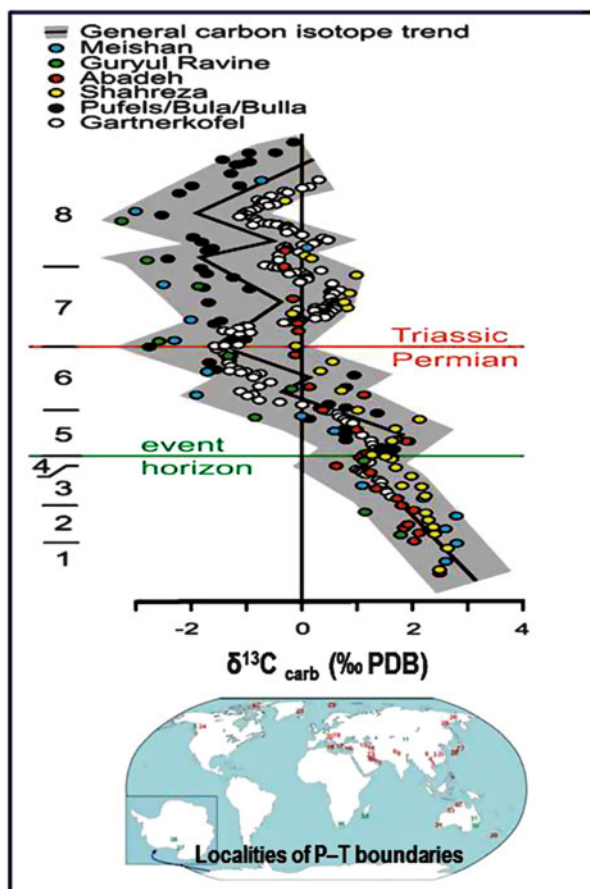


Fig. 2.10 General carbon-isotope trend across the P-T boundary constructed from the stratigraphically well-defined $\delta^{13}\text{C}$ data from Meishan, Guryul Ravine, Abadeh, Shahreza, Pufels/Bula/Bulla and the Gartnerkofel core. 1: *C. changxingensis*–*C. deflecta* Zone, 2: *C. zhangii* Zone, 3: *C. iranica* Zone, 4: *C. hauschkei* Zone, 5: *C. meishanensis*–*H. praeparvus* Zone (5+6: *H. praeparvus* Zone for shallow-water without *Clarkina* such as the Southern Alps), 6: *M. ultima*–*S.* 7: *H. parvus* Zone=Triassic part of *C. zhejiangensis* (for South Chinese intraplateau basins), 8= *I. isarcica* Zone (Korte and Kozur 2010; Elsevier, by permission)

of TOC and $\delta^{13}\text{C}$ anomalies across the K-T boundary in freshwater floodplains and swamp environments of Montana and Wyoming by Maruoka et al. (2007) reveal a marked decrease of $\delta^{13}\text{C}$ values by 2.6‰ (from -26.15‰ to -28.78‰) at Brownie Butte (Fig. 2.14), similar to the trend in carbonate at marine K-T sites. The $\delta^{13}\text{C}_{\text{org}}$ values are thought to reflect variations in carbon isotopes in atmospheric CO_2 in equilibrium with the ocean surface water. Other factors include enhanced contribution of organic matter derived from algae in a high-productivity environment due to

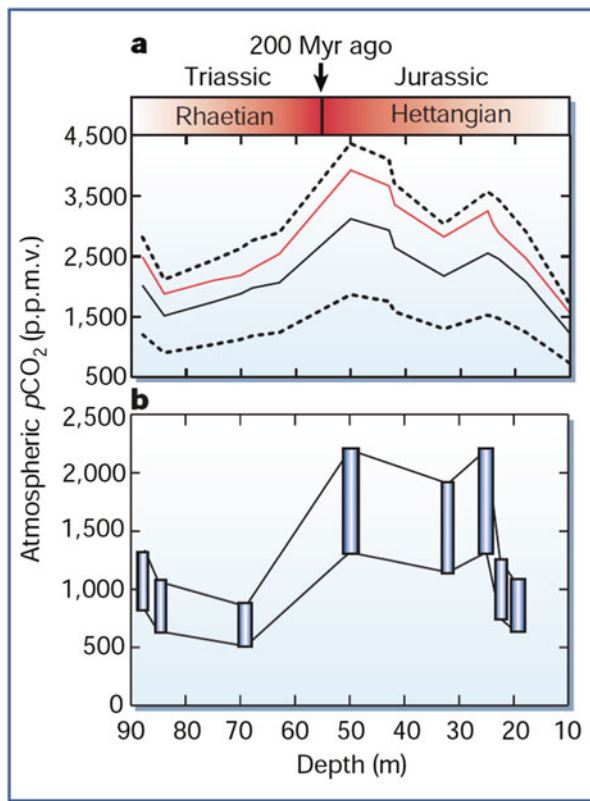


Fig. 2.11 Palaeo-atmospheric CO₂ variations across the Triassic–Jurassic boundary at 208 Ma. **(a)** Atmospheric CO₂ changes calculated using $\delta^{13}\text{C}$ values and a constant Triassic paleosol carbonate value up to the Triassic–Jurassic boundary and a constant Jurassic paleosol value; **(b)** Atmospheric CO₂ changes reconstructed from the stomata of fossil leaves. Vertical bars denote the upper and lower range for any given depth calculated using this technique (Beerling 2002a; Nature, by permission)

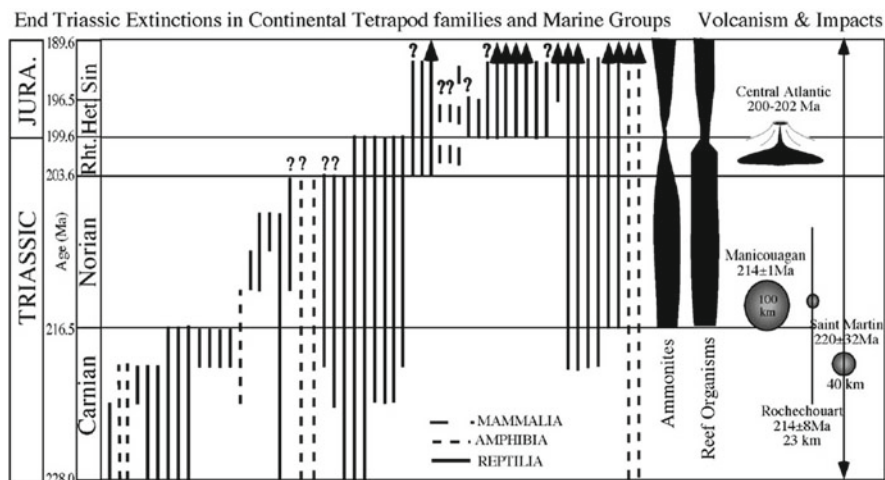


Fig. 2.12 Mass extinction, impacts and volcanism across the Triassic – Jurassic transition. Fauna changes modified after Hallam and Wignall (1997); volcanism after Courtillot and Renne (2003). (Keller 2005; Australian Journal of Earth Science, by permission)

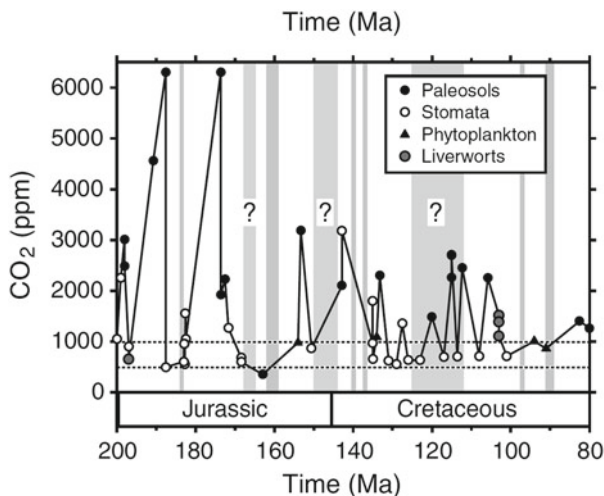


Fig. 2.13 CO₂ and temperature records for the Jurassic to late Cretaceous (~200–80 Ma). Cold periods with evidence for geographically widespread ice are marked with shaded bands. The horizontal dashed lines at 1000 and 500 ppm CO₂ represent the proposed CO₂ thresholds for, respectively, the initiation of globally cool events and full glacial periods (Royer 2006; Elsevier, by permission)

nitrogen fertilization and/or eutrophication induced by sulphide. The authors suggest the high productivity recorded in the K–T boundary clays imply that, by contrast to marine environments, freshwater environments re-recovered rapidly from the effects of impact. At a second K–T impact boundary site of Dogie Creek a positive shift of $\delta^{13}\text{C}_{\text{org}}$ is observed (Fig. 2.14) similar to other continental sites in North America. Variations between the sections suggest the effects of local environments such as anoxia and reactions with sulphide and sulphate related to acid rain effects of the impact.

Kaiho et al. (1999), reporting 36 isotopic analyses of K–T boundary samples from Caravaca, Spain, observe a rapid reduction in the gradient between $\delta^{13}\text{C}$ values in fine fraction carbonate and benthic foraminiferal calcite in sediments immediately above the K/T boundary, implying an abrupt extinction of pelagic organisms leading to a significant reduction in the flux of organic carbon to the seafloor. Variations in sulphur isotope ratios at Caravaca, Japan and New Zealand imply a rapid decrease in oxygen coincident with the $\delta^{13}\text{C}$ shift. A three-fold increase in the kaolinite/illite ratio and a 1.2‰ decrease in $\delta^{18}\text{O}_{\text{carb}}$ recorded in the basal 0.1–2 cm of Danian sediments indicate atmospheric and marine warming up to 3000 years following the $\delta^{13}\text{C}$ event. Recovery in the $\delta^{13}\text{C}_{\text{carb}}$ and commenced some 13,000 years kyr following the K–T event.

During periods when both asteroid impacts and volcanic eruptions occurred the respective roles of these events in driving mass extinctions is difficult to estimate

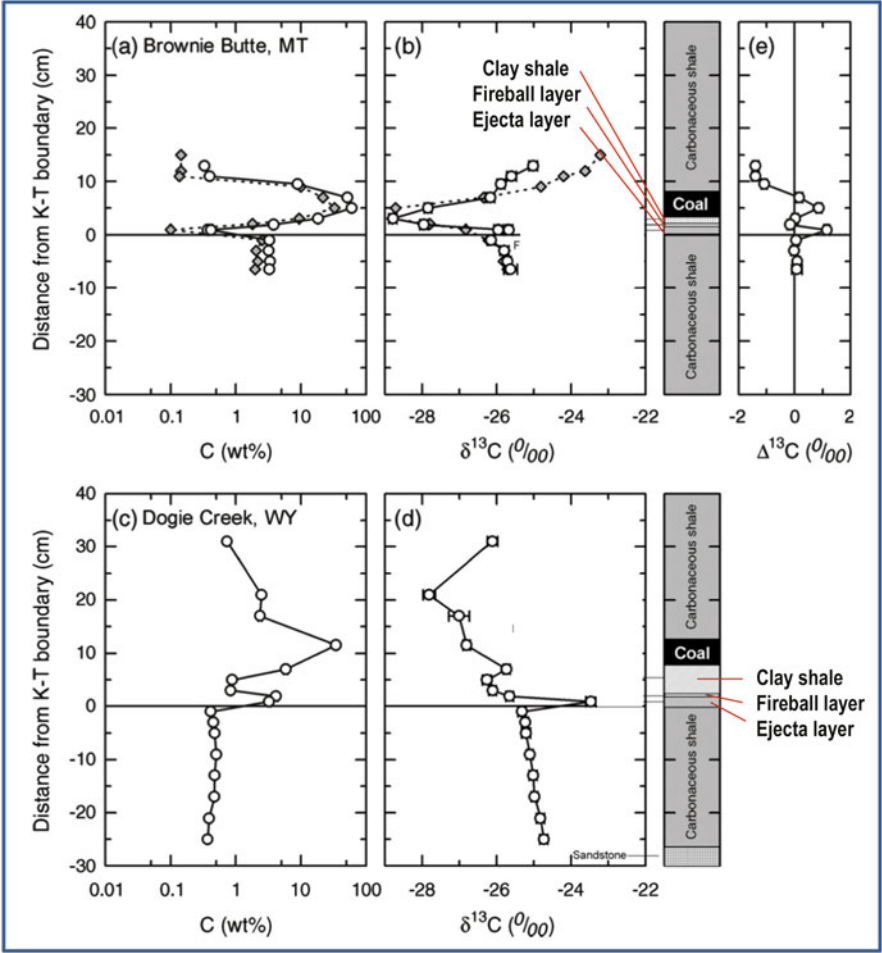


Fig. 2.14 Chemostratigraphic profiles for a organic carbon concentrations and b $\delta^{13}\text{C}$ values of bulk organic carbon for the Brownie Butte samples and for c organic concentrations and $\delta^{13}\text{C}$ values of bulk organic carbon for the Dogie Creek samples. *Open circles* and *gray diamonds* represent data obtained by Maruoka et al. (2007) and those obtained by Gardner and Gilmour (2002), respectively (Maruoka et al. 2007, Fig. 4; Elsevier, by permission)

and a relatively small number of asteroid impact structures have been accurately dated (Jourdan et al. 2012). The following temporal associations between volcanic and/or asteroid events and mass extinction are relevant (Fig. 2.1; Tables 2.1 and 2.2):

1. Acraman/Bunyerroo ~580 Ma asteroid impact and Acritarch radiation (Grey et al. 2003; Grey 2005) (Fig. 2.2).
2. Late Devonian (Frasnian-Famnenian) ~374 Ma Viley volcanism and mass extinction.

Table 2.1 Geological stage boundaries, large asteroid impact events, large volcanic provinces and percent mass extinction of species

Stage boundaries/ epochs	Large asteroid impacts	Large volcanic provinces	% Mass extinction of genera
Mid-Miocene Langhian 15.97 Ma	Ries (24 km) 15.1 ± 1.0 Ma	Columbia Plateau Basalt 16.2 ± 1 Ma	6
Eocene–Oligocene boundary 33.9 ± 0.1 Ma	Popigai (100 km) 35.7 ± 0.2 Ma; Chesapeake Bay (85 km) 35.5 ± 0.3 Ma Mount Ashmore: E-O Boundary	Ethiopian Basalts 36.9 ± 0.9 Ma	10
KT boundary 65.5 ± 0.3 Ma	Chicxulub (170 km) 64.98 ± 0.05 Ma Boltysh (25 km) 65.17 ± 0.64 Ma	Deccan Plateau Basalts. 65.5 ± 0.7 Ma (pooled Ar Ages: 65.5 ± 2.5 Ma)	46
Cenomanian–Turonian 93.5 ± 0.8 Ma	Steen River (25 km) 95 ± 7 Ma	Madagascar Basalts 94.5 ± 1.2 Ma	17
Aptian (Early Cretaceous) 125–112 Ma	Carlswell (39 km) 115 ± 10 Ma; Tookoonooka (55 km; 125 ± 1 Ma); Talundilly (84 km; 125 ± 1 Ma); Mien (9 km) 121 ± 2.3 Ma; Rotmistrovka (2.7 km) 120 ± 10 Ma	Ontong-Java LIP 120 Ma Kerguelen LIP 120–112.7–108.6 Ma Ramjalal Basalts, 117 ± 1	14
End-Jurassic 145.5 ± 4 Ma	Morokweng (70 km) 145 ± 0.8 Gosses Bluff (24 km) 142.5 ± 0.8 Ma; Mjolnir (40 km) 143 ± 2.6 Ma	Dykes SW India 144 ± 6 Ma	20
End-Pliensbachian 183 ± 1.5 Ma		Peak Karoo volcanism Start 190 ± 5 Ma; Peaks 193, 178 Ma; Lesotho 182 ± 2 Ma	19
End-Triassic 199.6 ± 0.3 Ma		Central Atlantic Igneous Province: 203 ± 0.7 to 199 ± 2 Ma Newark Basalts 201 ± 1 Ma	18
Norian/Rhatian 216.5	Manicouagan (100 km) 214 ± 1 Ma; Rochechouart (23 km) 213 ± 8 Ma;		34
Permian–Triassic: 251 ± 0.4 Ma; 251.4 ± 0.3 to 250.7 ± 0.3 Ma	Araguinha (40 km) 252.7 ± 3.8 Ma,	Siberian Norilsk 251.7 ± 0.4 to 251.1 ± 0.3 Ma	80
Late to end Devonian 374–359 Ma	Woodleigh (120 km) 359 ± 4 Ma; Siljan (52 km) 361 ± 1.1 Ma; Alamo breccia (~100 km) ~360 Ma; Charlevoix (54 km) 342 ± 15 Ma	Rifting and 364 Ma Pripyat–Dneiper– Donets volcanism	30 58
End-Ordovician 443.7 ± 1.5 Ma	Several small poorly dated impact craters		60
End-Early Cambrian 513 ± 2 Ma	Kalkarindji volcanic Province, northern Australia 507 ± 4 Ma		42

Table 2.2 Comparison of mean global temperature rise rates during the Cenozoic, including the K-T impact events (Beerling et al. 2002), the 55.9 Ma PETM hyperthermal event (Zachos et al. 2008), end-Eocene freeze and formation of the Antarctic ice sheet (34–32 Ma) (Zachos et al. 2001); Oligocene (Zachos et al. 2001), Miocene (Kurschner et al. 2008) and end-Pliocene (Zachos et al. 2001; Beerling and Royer 2011) thermal rises, glacial terminations (Hansen et al. 2007) Dansgaard-Oeschger cycles (Ganopolski and Rahmstorf 2002; Jouzel 2007), 8.2 kyr event (Wagner et al. 2002) intra-Holocene events (IPCC-AR4 2007) and Anthropocene climate change (IPCC-AR4 2007)

Age	Interval	Mean global land and sea temp change (C)	Warming rate (C/year)	CO ₂ change (ppm)	CO ₂ change rate (ppm/year)	Reference	Proxy methods
K-T impact 64.98 Ma	Instant to 10,000 years	Short freeze followed by ~+7.5C	~0.00075	~400 to 2300	Instantaneous to 0.19 ppm/yr	Beerling et al. 2002	Ginkgo stomata
PETM 54.9 Ma	~10,000 years	~ +5–9C	~0.0005	~1800 to 4000 ppm	~0.22 ppm/yr	Zeebe et al. 2009	Deep sea carbonate dissolution
Eo-Ol freeze 34.2–34.0	~200,000 years	~ -5.4C	-0.000027	~1120 to 560 ppm in 10 × 10 ⁶ years		Liu et al. 2009; Pollard and DeConto 2005	TEX86; δ18O of benthic foraminifera; Boron and alkenones model
End-Oligocene ~24.7	~200,000 years	~ +4C	0.00002	500–900 ppm	0.002	Pekar and Christie-Blick 2007	δ13C data from alkenones
Mid-Miocene 20–18 Ma	~200,000 years	~ +1.5C	0.000007	~300–520 ppm	0.0011	Kurschner et al. 2008	Multiple-species stomatal frequency record
End-Pliocene	4–3 Ma	~ +1C	0.000001	~250 to 400 ppm	0.00015	Zachos et al. 2001; Beerling and Royer 2011	Stomata pores; δ13C plankton
Glacial terminations/Eemian	11,000 years	+ ~5C	0.0004	+100 ppm	0.009	Hansen et al. 2007; Petit et al. 1999; EPICA 2004	Ice cores

(continued)

Table 2.2 (continued)

Age	Interval	Mean global land and sea temp change (C)	Warming rate (C/year)	CO ₂ change (ppm)	CO ₂ change rate (ppm/year)	Reference	Proxy methods
Dansgaard-Oeschger – 21 cycles of ~1500 years each	~75–15 kyr	~3.5C	0.01–0.2	+20 ppm	0.2	Ganopolski and Rahmstorf 2002; Jouzel 2007	Greenland ice cores
Younger dryas	12.9–11.7 kyr	~ –15C in GISP2 ice core		–7 ppm			Greenland ice cores
Interglacial stadial	~100 years	–3.3C in the North Atlantic		–25 ppm in ~300 years	–0.08	Wagner et al. 2002	Greenland ice cores
Medieval warm period (MWP)	~400 years	~0.4–0.5C	~0.001	5 ppm	~0.012	IPCC-AR4 2007 Chap. 4	Ice cores, tree rings, cave deposits
Little ice age (LIA)	~60 years	~ –0.4C	~ –0.006	–5 ppm		IPCC-AR4 2007 Chap. 4	Ice cores, tree rings, cave deposits
Post-1750	263 years	+0.9C +2.3C potential (with no aerosol masking)	~0.0034 ~0.008	280–400 ppm	~0.45	IPCC-AR4 2007	Instrumental
1975–2012	37 years	+0.6C	~0.016	330–394.28 ppm	~1.73	NASA/GISS IPCC-AR4 2007	Instrumental
March 2012–March 2013	1 year			2.89 ppm	2.89	NOAA 2013	

3. End-Devonian ~360 Ma impact cluster (Woodleigh, Siljan, Charlevoix, Alamo) and the destruction of reefs (McGhee 1996; Balter et al. 2008).
4. Permian-Triassic boundary ~251 Ma volcanic (Norilsk) and asteroid impact (Araguinha) events and mass extinction of species (Renne et al. 1995; Ross and Ross 1995; Wignall and Twitchett 1996; Twitchett et al. 2001; Racki 2003; Ward 2007).
5. Late-Triassic ~216 Ma impact (Manicouagan, Rochechouart) and mass extinction.
6. End-Triassic ~200 Ma opening of the Atlantic Ocean, extensive volcanism and extinction (Olsen and Sues 1986; McElwain et al. 1999; Jourdan et al. 2009; Whiteside et al. 2010)
7. Early Jurassic (Pliensbachian) ~183 Ma Karoo volcanism and extinction
8. End-Jurassic ~145 Ma impact cluster (Morokweng, Gosses Bluff, Mjolnir), opening of the Indian Ocean and extinction (McElwain et al. 1999).
9. Cretaceous-Tertiary boundary ~65 Ma impacts (Chicxulub, Boltish), Deccan volcanism and mass extinction.

2.1 Acraman Impact and Acritarchs Radiation

The ~580 Ma Acraman impact structure, estimated as ~90 km in diameter (Gostin et al. 1986; Gostin and Zbik 1999; Williams et al. 1996; Williams and Gostin 2005), and its ejecta layer found up to 550 km away from the crater, postdate the Marinoan glaciation (650–635 Ma). The impact was closely followed by radiation of Acritarch phytoplanktons, including an abrupt change from Ediacaran leiosphere palynoflora (ELP) to Ediacaran complex Acritarchs palynoflora (ECAP), presenting the oldest example of biological radiation following large catastrophic events (Grey et al. 2003; Grey 2005) (Fig. 2.2). The sequence from the terminal glacial sediments of the Cryogenian (~635 Ma) to the base Cambrian includes (1) cap carbonates, representing likely greenhouse gas-driven glacial collapse; (2) clastic sediments; (3) the ~580 Ma Acraman impact ejecta overlain by the Acritarchs-radiation horizon; (4) Ediacara fauna ~550 Ma (Fig. 1.14) and (5) ~544 Ma base Cambrian. The Acraman event is associated with marked negative $\delta^{13}\text{C}$ anomalies which signify increased deposition of organic matter (Calver 2000; Walter et al. 2000).

2.2 Cambrian and Late Ordovician Mass Extinction

The end-Ordovician period, marked by a glaciation about ~445.6–443.7 Ma and possibly longer (Frakes et al. 1992), saw two phases of extinction involving ~57 % of genera (Hallam and Wignall 1997), including pelagic graptolites and most benthic groups (trilobites, brachiopods, bryozoans, echinoderms) (Fig. 1.15).

Factors driving the extinction included cooling, glaciation, sea-level regression and major changes in oceanic circulation, leading to extinction of pelagic groups including graptolites and conodonts. The second phase appears to have been related to warming and ocean bottom anoxia eliminating shelf habitats (Hallam and Wignall 1997; Keller 2005). According to Kump et al. (1999) CO₂ levels declined during the glaciation from 5000 to 3000 ppm, high levels compensated by low insolation about 4 % lower than at present level of 342 Watt/m².

2.3 Late and End-Devonian Mass Extinctions

Possible factors associated with late Devonian mass extinctions include volcanism of the Viluy Traps, East European platform, estimated as >510,000 km³ and dated in the range 377 and 350 Ma (Keller 2005) (Fig. 2.1). The end-Devonian at ~360 Ma was marked by a large asteroid impact cluster including Woodleigh (D=120 km), Alamo (D=100 km), Charlevoix (D=54 km) and Siljan (D=52 km) and possibly Warburton East and Warburton West (D ~400 km) (Glikson et al. 2013). Devonian mass extinction events (McGhee 1996; Hallam and Wignall 1997) include a ~387 Ma extinction (~30 % of Genera) and ~374 Ma extinction (58 % of Genera) affecting pelagic fauna (Ammonoids, Cricoconoids, Placoderms, Conodonts, Agnathans) and benthic groups (Rugose corals, Trilobites, Ostracods and Brachiopods). The extinction involved collapse of Stromatoporoid reefs (Keller 2005). End-Devonian ~359 Ma extinction (~30 % of Genera) affected fish (Placoderms), ammonoids, conodonts, stromatoporoids, rugose corals, trilobites and ostracods. Major factors included ocean anoxia, declining biological activity (high $\delta^{13}\text{C}$), and warming (low $\delta^{18}\text{O}$) (Balter et al. 2008). The late Devonian mass extinctions are superposed on a protracted cooling trend associated with a decline in CO₂ levels from a range of ~3200–5200 ppm to below ~500 ppm. Concomitant decline in $\delta^{13}\text{C}$ from ~22 to ~15‰ from ~405 Ma to 280 Ma is indicated by paleosols (Mora et al. 1996). The development in the Late Devonian of plant megaphyll leaves with their branched veins containing high stomata density allowed vegetation to adapt to the cool low-CO₂ conditions of the Carboniferous-Permian (Rothwell et al. 1989; Beerling et al. 2001).

2.4 Late Permian and Permian-Triassic Mass Extinctions

Major eruptions of the Siberian Norilsk magmatic province and Emeishan volcanism (Renne et al. 1995; Wignall and Twitchett 1996; Wignall 2001) about ~251 Ma (251.7±0.4 to 251.3±0.3 m.y., Kamo et al. 2003) and a large asteroid impact (Araguinha, Brazil, D=40 km, ~247.8±3.8 Ma; Tohver et al. 2012), which excavated carbonates and shale (Table 2.1), has led to a rise of atmospheric CO₂ levels to ~3400 ppm (Royer 2006) (Fig. 2.8), associated with the greatest mass extinction recorded in geological history (Figs. 2.9 and 2.10).

Two major extinction phases are defined:

- A. ~50 percent of genera extinguished at the ~260 Ma Late Permian Maokouan Stage. Tropical zones saw the extinction of echinoderms, corals, brachiopods, sponges, fusulinid foraminifera and ammonoids (Ross and Ross 1995; Keller 2005) (Table 2.1; Fig. 2.9).
- B. ~78 percent of genera extinguished at the ~251 Ma end-Permian Changhsingian Stage, effecting abrupt extinction of the Rugose Corals, Bryozoans, complex Foraminifera, many Gastropod and Bivalve families, radiolarians and many Ammonoid families (Hallam and Wignall 1997; Racki 2003) (Table 2.1, Fig. 2.9).

The two events were separated by the Capitanian and Wuchiapingian Stages (265.8–253.8 Ma) (Keller 2005). An abrupt nature of these events is indicated by their short duration of 10–50.10³ years and negative $\delta^{13}\text{C}$ excursion indicating deposition of fauna and flora remains (Twitchett et al. 2001). Nektonic (free swimming) fauna, including fish, conodonts and nautiloids survived better thanks to their mobility in the upper water column above anoxic bottom water (Keller 2005). Anoxia is evidenced by sulphide-rich and black clay sediments and negative $\delta^{13}\text{C}$ anomalies testifying to mass settling of organic matter. Grasby et al. (2011) suggested a link between extinction and a release of carbon ash/char derived from the combustion of Siberian coal and organic-rich sediments by flood basalts, which was dispersed globally and created toxic marine conditions.

Berner (2005) investigated geochemical trends across the Permian-Triassic boundary from isotopic $\delta^{13}\text{C}$ and $\delta^{34}\text{S}$ mass balance and estimates of weathering and burial of carbon and sulphur. A drop in the rate of organic burial from the late Permian to the mid-Triassic is attributed to rising aridity and decrease in biomass due to a transition from forests to herbaceous grassland. A major drop in oxygen from 30 % to 13 % was associated with an increase in the ratio of pyrite to organic carbon and in development of marine euxinic basins. Consequences included extinction of vertebrates and loss of giant insects and amphibians. According to Ward (2007) ocean acidification due to rising CO_2 levels, polar ice melt, reduced ocean current system and the conveyor belt which provides oxygen, consequent anoxia, production of H_2S by sulphur-reducing microbes and its release to the atmosphere, constituted critical factors in sea and land mass extinction.

2.5 End-Triassic Mass Extinction

The opening of the Central Atlantic magmatic province by the end-Triassic at ~200 Ma, involving copious basaltic volcanism (Hames et al. 2003; Courtillot and Rennes 2003; Jourdan et al. 2009) affected a major mass extinction event represented by a large negative carbon isotope excursion, reflecting perturbations of the carbon cycle including an increase in CO_2 (Beerling 2002a; Whiteside et al. 2010) (Fig. 2.11). The end-Triassic was preceded by a Norian (~216–213 Ma) extinction associated with the large Manicouagan impact ($D \sim 100 \text{ km}$; $214 \pm 1 \text{ Ma}$) (Table 2.1).

The extinction affected ammonites, which radiated back in the early Jurassic, reef organisms, conodonts and bivalves, as well as a crisis in terrestrial plants (Hallam and Wignall 1997; Keller 2005) (Fig. 2.12). The duration of the extinction is variously estimated as between 50 and 200 kyr (Olsen and Sues 1986). According to Beerling (2002a), depending on the proxy used, CO₂ levels rising from the Rhaetian (~204 Ma) reached about ~1300–2200 from leaf stomata and a wider range from carbon isotopes, just above the Rhaetian-Hettangian (early Jurassic) boundary (Fig. 2.11), signifying an extreme greenhouse event of ~34 % of genera.

2.6 Jurassic-Cretaceous Extinction

The Triassic-Jurassic boundary marks a major faunal mass extinction (Fig. 2.13), but records of accompanying environmental changes are limited. Paleobotanical evidence across the boundary indicates a marked increase in atmospheric CO₂ and associated temperature rise of 3–4 °C. These environmental conditions are calculated to have raised leaf temperatures above a highly conserved lethal limit, perhaps contributing to the >95 % species-level turnover of Triassic-Jurassic megaf flora (McElwain et al. 1999).

2.7 K-T (Cretaceous-Tertiary Boundary) Mass Extinction

The K-T boundary (64.98 ± 0.05 Ma) marks the second largest mass extinction of species recorded in Earth history, when some 46 per cent of living genera disappeared (Keller 2005, 2012) (2.1, 2.15, 2.16, 2.17). Alvarez et al. (1980) discovered a hiatus across the Cretaceous-Paleocene boundary in Italy, where a foraminifera-rich white limestone facies containing large-scale *Globotruncana contusa* is abruptly replaced by overlying clay-rich red limestone termed Scaglia rossa containing smaller foraminifera (*Globigerina eugubina*) and micron-scale algal coccoliths (Fig. 2.17). At the classic locality at Gubbio a ~1 cm-thick boundary clay layer consisting of a lower ~5 mm-thick grey clay zone consists of clastic material and an upper ~5 mm-thick red clay zone termed ‘fire layer’. This layer contains an Iridium anomaly of up to ~9 ppb and similar relations are observed elsewhere (Figs. 2.15, 2.16, and 2.17). The boundary coincides with a major geomagnetic reversal correlated with a marine magnetic anomaly sequence dated with foraminifera. The parent craters of the K-T event have been identified, including Chicxulub (170 km in diameter, Yucatan Peninsula, Mexico) and Boltysh (~25 km in diameter; 65.17 ± 0.64 Ma, Ukraine). Since the initial discovery of K-T impact ejecta, best preserved in deep water environment, 101 sites have been identified along the Maastrichtian – Danian boundary around the globe (Claeys et al. 2002). Around the Gulf of Mexico and the Atlantic Ocean the ejecta layer coincides with erosion of Maastrichtian sediments and is overlain by clastic sediments and breccia attributable to seismic and tsunami effects.

A panel of 41 international experts from 33 institutions concluded the evidence for a cause and effect relation between asteroid impact and mass extinction at the

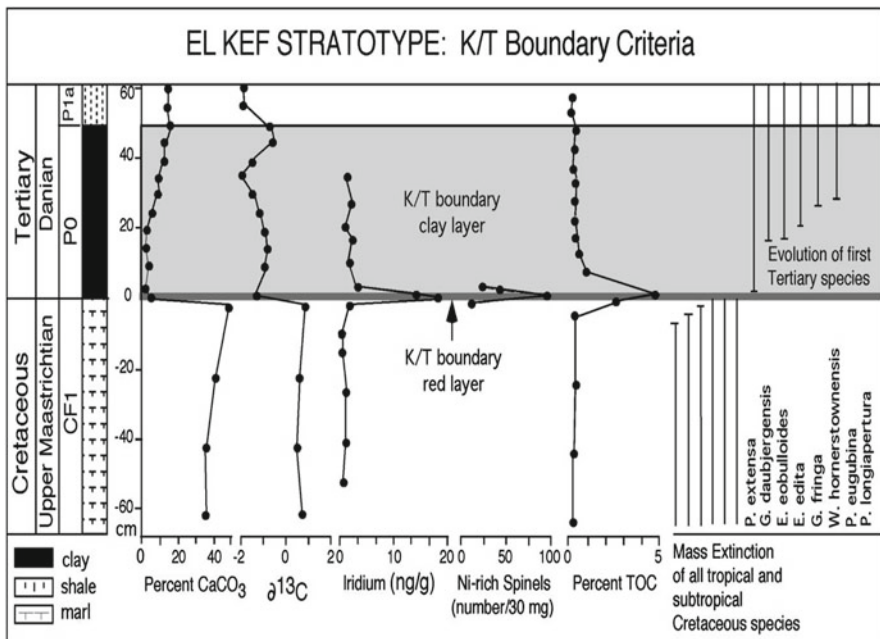


Fig. 2.15 K/T boundary at the El Kef, Tunisia, defined by a dark organic-rich boundary clay with thin red layer at its base (see fig. 2.17) enriched in iridium, nickel rich spinels, pyrite and rare clay spherules, a negative $\delta^{13}\text{C}$ excursion, high Total Carbon Contents (TOC) and low CaCO_3 , and extinction of tropical and subtropical species (Keller 2005; Australian Journal of Earth Science, by permission)

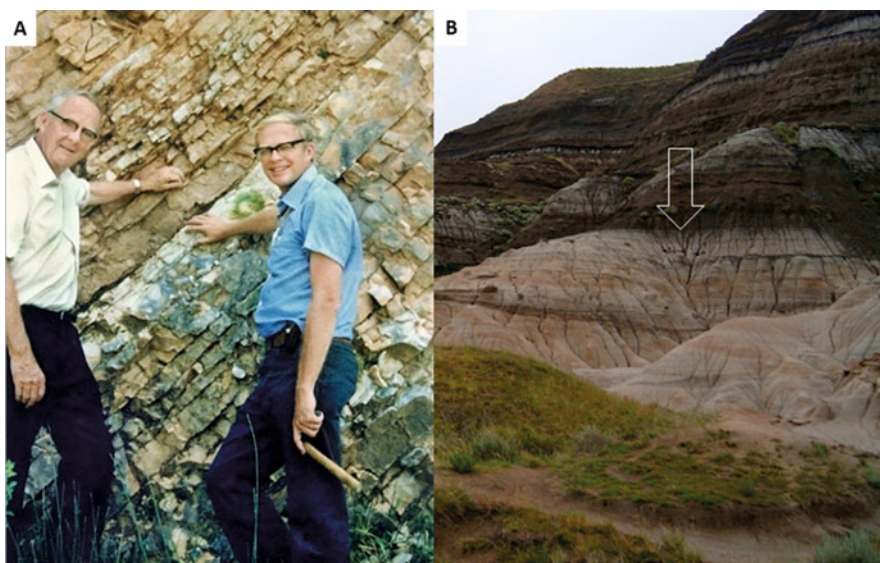


Fig. 2.16 (a) Walter and Luis Alvarez at the KT boundary at Gubbio. http://en.wikipedia.org/wiki/Luis_Walter_Alvarez#mediaviewer/File:LWA_with_Walt.JPG; (b) the KT boundary near Drumheller, by Glen Larson. Wikipedia Commons. http://commons.wikimedia.org/wiki/File:KT_boundary_054.jpg

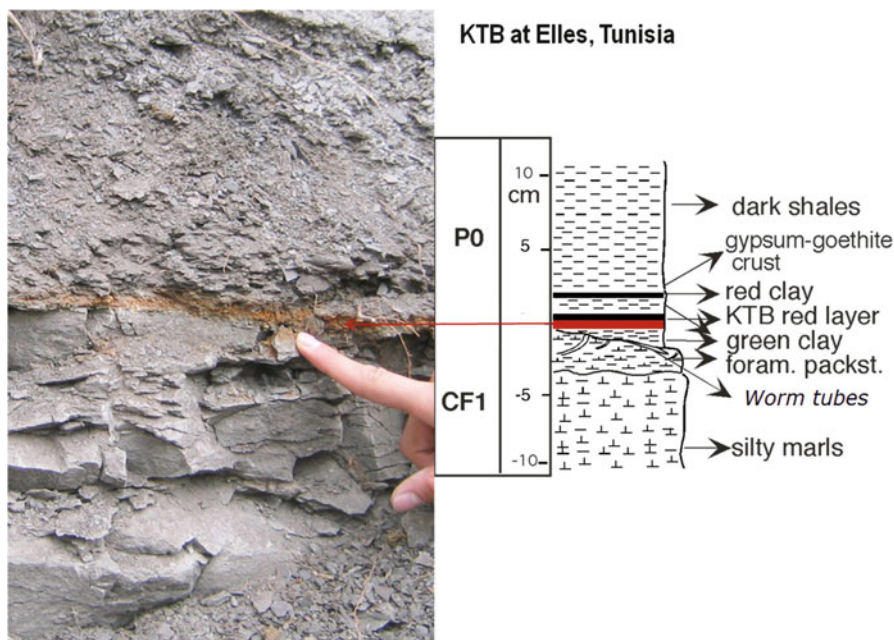


Fig. 2.17 The K/T boundary at Elles, Tunisia (Courtesy G. Keller)

K-T boundary is overwhelming (Schulte et al. 2010). The Chicxulub impact and Boltysh impacts occurred during an active volcanic period which saw continuing eruptions in the Deccan (northwest India) volcanic province recently dated by U-Pb ages (Schoene et al. (2015) to have commenced approximately ~250,000 years before the K-T boundary. The Deccan volcanism produced >1.1 million km³ of basalt during ~750,000 years, inducing environmental changes preceding the terminal effects of the extraterrestrial bombardment. Stomata leaf pore-based estimates of atmospheric CO₂ during these events indicate an abrupt rise from ~350–500 ppm to at least ~2300 ppm within about 10,000 years, consistent with instantaneous transfer of ~4,600 Gigaton Carbon (GtC) to the atmospheric reservoir. Climate models suggest consequent forcing of 12 Watt/m², sufficient to warm the Earth's surface by ~7.5 °C in the absence of counter forcing by sulphate aerosols (Beerling et al. 2002). According to these authors a CO₂ rise of ~1800 ppm and temperature rise occurred over a period of ~10,000 years, namely at rates of ~0.18 ppm/year and 0.00075 °C/year.

Short term effects of the K-T asteroid impact include incineration of large land surfaces from the heat pulse of the incoming projectile, from the explosion and settling of ejecta and microkrystite spherules (Wolbach et al. 1990), ejection of dust and water vapor and oxidation of atmospheric nitrogen and consequent ozone depletion. Longer term effects included release of CO₂ and other greenhouse gases with consequent warming, ocean acidification and anoxia (McCracken et al. 1994; Covey et al. 1997). The K-T mass extinction involved phytoplankton, calcareous

nanoplankton, planktonic foraminifera, benthic foraminifera, 54 % of diatoms, marine invertebrates, crustaceans, ostracods, 98 % of tropical colonial corals, 60 % of late Cretaceous Scleractinia coral, echinoderm, and bivalve genera, numerous species of the molluscan and Cephalopoda and all cephalopod species, belemnoids and ammonoids, 35 % of echinoderm genera, rudists (reef-building clams), inoceramids (giant relatives of modern scallops), jawed fishes, cartilaginous fishes. Survivors included approximately 80 % of the sharks, rays, and skates families. In North America, approximately 57 % of plant species became extinct. All Archaic birds and non-avian dinosaurs became extinct. Cretaceous mammalian lineages, including egg-laying mammals, multi-tuberculates, marsupials and placentals, dryolestoids, and gondwanatheres survived. Marsupials mostly disappeared from North America and Asian deltatheroidans became extinct. Many of these extinctions constituted proximal instantaneous consequences of the fire ball and asteroid explosion, while distal habitats were affected by more protracted consequences.

2.8 Paleocene-Eocene Extinction

The Paleocene-Eocene thermal maximum (PETM) at ~55.9 Ma involved a release of some ~2000 billion ton carbon (GtC) as methane, elevating atmospheric CO₂ to near-1800 ppm at a rate of 0.18 ppm/year, and mean temperature rise of ~5 °C (Zachos et al. 2008; Panchuk et al. 2008; Cui et al. 2011). Elevated CO₂ led to acidification of ocean water from ~8.2 to ~7.5 pH and the extinction of ~35–50 % of benthic foraminifera during a period of ~1000 years (Zachos et al. 2008). Other consequences included a global expansion of subtropical dinoflagellate plankton, appearance of modern orders of mammals, including primates, a transient dwarfing of mammalian species, and migration of large mammals from Asia to North America.

2.9 The End-Eocene Freeze

The incidence of an asteroid impact cluster about 35.7–35.6 Ma (Popigai, Siberia ~100 km-diameter; Chesapeake Bay, off-shore Virginia – 85 km-diameter; Mount Ashmore, Timor Sea – >50 km-diameter; the related North American strewn tektite field) and the abrupt decline in temperatures about ~33.7–33.5 Ma can be expected to have triggered major environmental and biotic transformations. Abrupt cooling (Pearson et al. 2009) was associated with elimination of warm-water planktonic species (Keller 1986, 2005). Alvarez (2003) and Poag (1997) suggested impact-related extinctions during the late Eocene and the E-O transition, whereas Keller (2005) ruled out impact-triggered extinction. Isotopic $\delta^{13}\text{C}$ and $\delta^{18}\text{O}$ studies of late Eocene Iridium-rich ejecta layers at Massignano, Italy, indicate increase in temperature and in organic matter associated with the impacts, possibly reflecting release of methane hydrates by impact excavation (Monechi et al. 2000; Bodiselsitch et al. 2004).

Climate, Fire and Human Evolution

The Deep Time Dimensions of the Anthropocene

Glikson, A.Y.; Groves, C.

2016, XVIII, 227 p., Hardcover

ISBN: 978-3-319-22511-1